12th International Workshop on Simulation for Energy, Sustainable Development & Environment, 005
21st International Multidisciplinary Modeling & Simulation Multiconference

2724-0061 © 2024 The Authors.
doi: 10.46354/i3m.2024.sesde.005

Optimization of Implantation and Diffusion Parameters to Minimize the Point Defects Formation in Textured Thin Film Solar Cells

Abderrazzak El Boukili[1,*]

[1]Al Akhawayn University in Ifrane, P.O. Box 104, Avenue Hassan II, 53000, Morocco

[*]Corresponding author. Email address: a.elboukili@aui.ma

Abstract

The goal of this paper is to understand how to minimize the crystal point defects caused by boron ion implantation in a textured thin film silicon solar cell. The defects control the performance of any device. It is well known that point defects are responsible for the recombination losses in any solar cell. Understanding how to minimize point defects will help minimize these recombination losses and maximize the efficiency of the solar cells. Using accurate simulations and advanced pair-diffusion models, we investigated quantitatively the relation between different values of ion implantation parameters, ion diffusion parameters and the maximum amount of the remaining point defects after annealing. Firstly, we found that the densities of point defects depend more on the diffusion temperatures, T, than on the ion implantation doses. Secondly, we discovered that the remaining interstitial and vacancy defects have been reduced from 10^{22} to 1.02 and from 10^{22} to 1.09×10^{9}, respectively, when a diffusion with an optimal high temperature T_{OH} is followed by a diffusion with an optimal low temperature T_{OL}. We think that this is a breakthrough. The obtained results for dopant profiles and junction depths are in good agreement with experimental and theoretical results found in recent literature.

Keywords: Optimization, point defects; simulation, textured, thin film solar cells

1. Introduction

The main goal of this paper is an attempt to learn, understand and investigate how to minimize the amount of the non-equilibrium point defects that will still exist after the boron thermal diffusion in an N-type textured thin film crystalline silicon solar cell.

It is very well known that the non-equilibrium point defects or dislocation loop defects that will stay in the solar cell after diffusion will cause Auger recombination losses and resistive losses of the photogenerated carriers in the solar cell. These losses will significantly reduce the efficiency of the cell (Jan et al., 2022) (Lucio et al., 2019) (Savita et al., 2019).

For example, the efficiencies of modules sold in 2021 typically range from 17.4% (low-grade multi-crystalline cells) to 22.7% (high-performance back-contacted cells) with an estimated average of 20% for the most produced technology (passivated emitter and rear cell, PERC and monocrystalline silicon solar cells) (Jan et al., 2022). Then, about 80% of the solar energy

is lost by the most recent silicon solar cells found in the market. The point defects are the main contributors to this 80% loss.

To the best of our knowledge, an investigation to quantify and understand how to minimize the point defects after boron thermal diffusion in an N-type textured silicon solar cell is still missing in published literature. The defects control the performance of any device. Using accurate two-dimensional simulations and advanced pair-diffusion models, we investigated quantitatively the relation between different values of implantation doses, annealing times, annealing high and low temperatures, and the maximum amount of point defects that exist after annealing.

To calculate accurately the maximum amount of point defects induced by ion implantation damage, we used the open-source two-dimensional process simulator Suprem-IV (Hansen et al., 1993) and the analytical model of Gerhard and Siegfried (Gerhard et al. 1988).

The maximum amount of point defects calculated is in order of 10^{22} atoms per square centimeter, after ion implantation.

After thermal diffusion, we firstly found that the densities of point defects depend more on the diffusion temperatures, T, than on the ion implantation doses. Secondly, we found that the interstitial and vacancy defects have been reduced from 10^{22} to 4.3×10^{13} and from 10^{22} to 4.8×10^{15}, respectively, after a thermal diffusion using an optimal high temperature T_{OH} given by: $T_{OH}=950°C$. We define an optimal high temperature, T_{OH}, to be a temperature for which all the dopants are activated, the desired junction depth is reached, and the amount of non-equilibrium point defects is less than the amount of equilibrium point defects. Based on our numerical experiments, we believe that for any given set of implantation and diffusion parameters, we can find an optimal high temperature T_{OH}.

Thirdly, we discovered that the process where a thermal diffusion with an optimal high temperature T_{OH} is followed by a thermal diffusion with an optimal low temperature, T_{OL}, given by: $T_{OL}=100°C$, has further reduced the remaining interstitial and vacancy defects from 4.3×10^{13} to 1.02 and from 4.8×10^{15} to 1.09×10^{9}, respectively. Another good news is that after this process, the dopant profile and junction depths were unchanged. We think that this discovery is a breakthrough. We invite others to run laboratory experiments to double check these key findings coming from the numerical experiments in this paper. Unfortunately, we do not have access to laboratory experiments.

On the other hand, the obtained results for dopant profiles and junction depths are qualitatively and quantitatively in good agreement with experimental and theoretical results found in recent literature for similar devices.

2. State of the art

In photovoltaic silicon solar cells, many different types of crystal defects may exist. The most common crystal defects are point defects, line defects or dislocations loops, plane defects, and volume defects or clusters and precipitates (Jan et al., 2022) (Savita et al. 2019) (Krugener et al., 2014). The point defects are made up of interstitial defects (I) and vacancy defects (V) as shown in Figure 1.

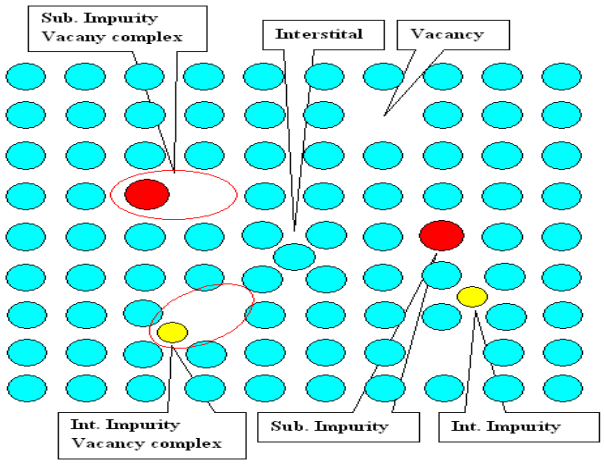

Figure 1. Possible types of point defect complexes in a silicon solar.

The equilibrium point defects are created during the fabrication processes of the silicon raw material. Equilibrium point defects can be also found in a pure monocrystalline silicon material. Not everything in life is perfect.

The densities of the equilibrium point defects C^*_I and C^*_V depend strongly on the growth temperatures of the silicon material.

The non-equilibrium point defects are created during the fabrication processes of the devices as photovoltaic silicon solar cells (Hao et al., 2022) (Adeline et al., 2019) (Krugener et al., 2014).

The boron ion implantation is the method of choice to fabricate the emitter and the pn-junction of an N-type textured silicon solar cell (Meyer et al., 2021)(Savita et al., 2019) (Adeline et al., 2019) (krugener et al., 2014), see Figure 2.

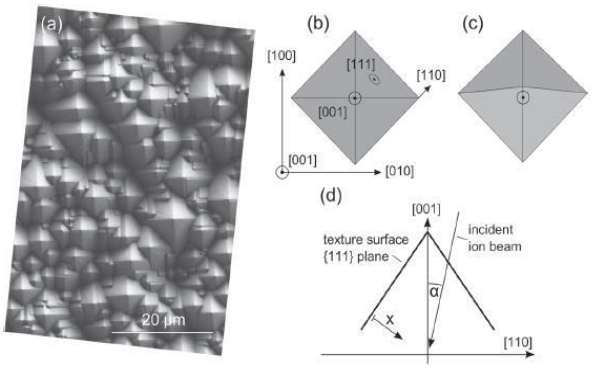

Figure 2. SEMS images of random pyramids for a textured solar cell (Krugener et al., 2014). Sharp Tips and Valleys of the pyramids are visible in the left image.

Most of the non-equilibrium point defects are caused by the ion implantation induced damages (Jan et al., 2022) (Tavita et al., 2020).

Their densities C_I and C_V depend significantly on the ion implantation parameters as: ion implantation dose, energy, ion beam tilt, screening oxide, angle of rotation of the cell, types of the dopant species, and pressure (Jan et al., 2022) (Savita et al., 2019) (Liang et al., 2015) (Krugener et al., 2014) . On the other hand, some non-equilibrium point defects can be created during dopant thermal diffusion processes. Another more complicated concern is that during high temperature thermal diffusion processes some point defects may give birth to more complex defects as dislocation loops' defects, cluster defects or precipitates (Jan et al., 2022) (Liang et al., 2015) (Krugener et al., 2014).

Ion implantation in upright pyramidally textured PERC solar cells has been discussed in (Savia et al., 2022). Aging induced degradations in silicon solar cells has been investigated in (Rahman et al., 2023). Retarded boron and phosphorus diffusion in silicon nanopillars due to stress induced vacancy defects injection has been investigated in (Jan et al., 2022). Boron diffusion profiles in N-type textured monocrystalline silicon solar cells based on plasma-enhanced chemical vapor deposition method (PECVD) have been discussed in (Hao et al., 2022). In (Krugener at al., 2014), transmission electron microscopy (TEM) images have been performed to see and measure experimentally the dislocation loops defects that will still exist after boron diffusion in a textured Si(001) bulk solar cell. They observed a higher density of dislocation loops defects on the valleys between the pyramids compared to other locations close to the textured surface of the solar cell. After 15mn annealing when T=900°c and the implantation dose is 1.7×10^{15} atoms per square centimeter, the measured density of dislocation loops defects was 1.7×10^{10} (Krugener et al., 2014). A similar amount of measured dislocation loops defects on planar surfaces (about 7×10^{9}) has been shown in (Liu, 1996).

Liang et al. (2015) used X-ray diffraction measurement of the crystallographic quality of the implanted regions and showed that a higher implantation dose would result in a degradation of crystallographic quality after annealing. They also found that low annihilation temperatures are insufficient to cure the residual defects created during the high dose implantation processes.

Based on the published literature we have investigated, we found that the exact amount of all types of defects created after ion implantation and subsequent thermal diffusion is still unknown. Since this is a challenging and complex problem in solar energy and opto-electronics industries. The knowledge of this amount of defects can help optimize the diffusion processes, enhance the silicon solar cells efficiency and help ion implantation technology to compete with other doping techniques. In this paper, we are attempting to first identify quantitatively the amount of point defects (Interstitials (I) and Vacancies (V)) that will exist after boron thermal diffusion in a textured N-type silicon solar cell. In future work, we will concentrate on the line defects coming from dislocation loops.

This paper is organized as follows. Section 2 outlines the analytical models we are using to calculate accurately the amount of point defects we get right after the boron ion implantation. Section 3 presents the main Equations of the pair-diffusion models we are solving to accurately estimate the amount of point defects that will remain after thermal ionic diffusion of boron dopant ions, interstitial ions, and vacancy ions. In this paper, we are using the pair-diffusion model where the diffusion flux of the interstitial defects is added to the diffusion flux of the boron dopant ions. We are using the open source two-dimensional process simulator Suprem-IV to solve the system of six coupled partial differential Equations rising from the pair-diffusion model (El Boukili 2019) (Hansen et al., 1993). Section 4 presents and analyzes the numerical results obtained from the application of the presented models in Sections 2 and 3. A qualitative and quantitative comparison of the obtained results with literature is presented as well for the remaining point defects and the activated boron dopant. Section 5 summarizes the concluding thoughts and future work.

3. Accurate models to calculate the densities of point defects after Ion implantation

To calculate accurately the amount of point defects that exist right after ion implantation in the textured solar cell sample we are working on, we use the two-dimensional model of Gerhard and Siegfried (Gerhard et al. 1988). This model is implemented in Suprem-IV. In this model, the point defect concentrations $C_I^0(x,y)$ and $C_V^0(x,y)$ for interstitial defects and vacancy defects, respectively, are calculated using a combination of an exponential function and a Gaussian function. Here x and y represent the lateral and vertical dimensions as shown in **Figure 1**. For ion implantation technologies using light ions such as boron ions that we are using in this paper, the point defect concentrations, right after ion implantation, are given by:

$$\begin{aligned} C_I^0(x,y) &= f_I(y)\times g_I(x,y) \\ C_V^0(x,y) &= f_V(y)\times g_V(x,y) \end{aligned} \quad (1)$$

Where:

$$f_I(y) = \begin{cases} C_1 \exp(\frac{y}{a_1}) & \text{if } z \le z_0 \\ C_2 \exp(-\frac{(z-a_2)^2}{2a_3^2}) & \text{if } z \ge z_0 \end{cases} \quad (2),$$

and $g_I(x,y)$ is a Gaussian function. The same models are used for $f_V(y)$ and $g_V(x,y)$. The parameters $C_1, C_2, a_1, a_2, a_3, z_0$ are calculated by fitting the analytical functions $C_I^0(x,y)$ and $C_V^0(x,y)$ to Monte Carlo results (Gerhard et al., 1988). These models have been validated in (Gerhard et al., 1988) for boron and arsenic ion implantation in a planar silicon material with a mask edge on the top surface. In this paper, we are extending the application of these models to a pyramidally textured silicon solar cell. We are expecting the texturing to cause some singularities to these analytical functions and their derivatives. In this paper, we are extending the application of these models to a pyramidally textured silicon solar cell. We are expecting the texturing to cause some singularities to these analytical functions and their derivatives. In this paper, the point defect concentrations $C_I^0(x,y)$ and $C_V^0(x,y)$ are used as the initial values of the total point defect concentrations $C_{TI}(x,y,t)$ and $C_{TV}(x,y,t)$ that remains after thermal atomic diffusion at time t. On the other hand, to calculate accurately the boron dopant concentration, $C_B^0(x,y)$, we get right after ion implantation, we use Pearson-IV analytical model (El Boukili 2019: SESDE). The boron dopant concentration, $C_B^0(x,y)$, is used as the initial value of the total boron dopant concentration, $C_{TB}(x,y,t)$, we get after thermal atomic diffusion at time t.

4. Advanced pair-diffusion models to estimate the remaining densities of point defects after thermal atomic diffusion

The main step, in the fabrication processes of a solar cell, that comes after ion implantation is the thermal atomic diffusion of dopants and point defects. Thermal atomic diffusion is mainly used to activate the dopants (A), move the dopants to the desired depth, and cure the defects induced by the ion implantation processes. Atomic thermal diffusion depends on so many parameters. In the present study, we investigate the two main diffusion parameters which are temperature, T, and time t. Humans use time and temperature to cure their problems. Solar cells do the same thing.

When we heat up a solar cell with a temperature T and for a period of time t, the dopants (A) and the point the defects I or V will diffuse as a pair using different pair diffusion mechanisms as shown in Figure 3. You could see (El Boukili 2019) for more details. According to literature, some dopants (A) diffuse with interstitials (I), some diffuse with vacancies (V), and some diffuse with both interstitials and vacancies [14], [15], [16], [17], [18], IRSEC 2019: Diffusion.

In this study, we assume that boron dopants diffuse only as a couple with interstitials. This assumption is used in many recent published papers [14], [15], [16], [17], [18], IRSEC 2019: Diffusion. This assumption will impact the mathematical models we are going to use for the boron diffusion fluxes and the boron diffusion coefficient ($D_B(x,y,T)$). Let $C_{TB}(x,y,t)$ be the total dopant concentration we get after the thermal atomic diffusion at time t.

To calculate accurately $C_{TB}(x,y,t)$, $C_{TI}(x,y,t)$ and $C_{TV}(x,y,t)$ concentrations, we use an advanced pair-diffusion model from Suprem-IV (Hansen et al., 1993).

In a pair-diffusion model, some dopant ions (A) are free and some other dopant ions (AI or AV) are married to point defects I or V. Free dopant ions (A) are always assumed to be immobile. They do

not diffuse. On the other hand, the married dopant ions (AI or AV) can't diffuse on their own. They need the neighboring point-defects I or V as diffusion vehicles as shown in Figure 2. When a binding energy between a dopant impurity (A) and a neighboring defect I or V is not weak, the impurity (A) and the point defect I or V will move as a pair impurity-defect AI or AV until they get separated by recombination or other factors. To the contrary of the dopant ions (A), some point defects I and V can diffuse as free point defects and some can diffuse as a pair AI or AV with dopants (A).

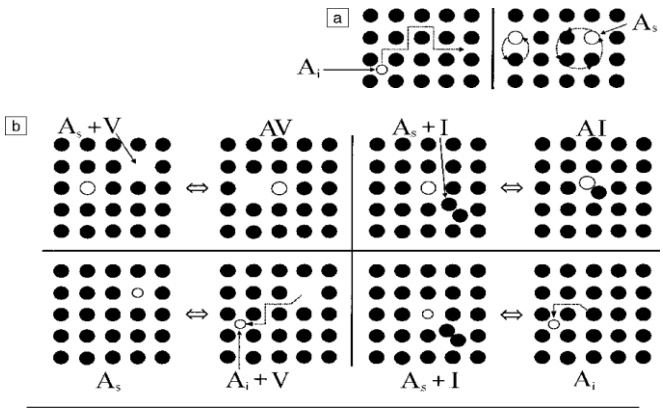

Figure 3: Paired diffusion mechanisms.

A dopant (A) is either at a substitutional site (A_s) on the silicon crystal or at an interstitial location (A_i). We have:

$$C_{TB} = C_B + C_{BI} + C_{BV} \quad (3)$$

$$C_{TI} = C_I + C_{BI} \quad (4)$$

$$C_{TV} = C_V + C_{BV} \quad (5)$$

Where $C_B(x,y,t)$, $C_I(x,y,t)$, and $C_V(x,y,t)$ are the concentrations of the unpaired (free) dopants (B), interstitials (I) and vacancies (V), respectively. The $C_{BI}(x,y,t)$, and $C_{BV}(x,y,t)$ are the concentrations of the paired dopants (BI or BV) or the paired interstitials (BI) or the paired vacancies (BV).
The diffusion model we are solving using Suprem-IV involves 6 coupled partial differential equations of second order for the six species: electrostatic potential $\varphi(x,y)$, B, BI, BV, I, V. The first Equation is the Poisson's Equation. The second Equation is the diffusion Equation for the free dopant ions B. The third and the fourth Equations represent the pair-diffusion Equations of dopant ions with interstitial (AI) and with vacancy ions (AV). The fifth Equation represents the diffusion Equation of the free interstitial defects I. The sixth Equation represents the diffusion Equation of the free vacancy defects V. The six unknowns of this diffusion model are: the electrostatic potential $\varphi(x,y)$ and the 5 coupled concentrations: $C_B(x,y,t), C_I(x,y,t), C_V(x,y,t)$, $C_{BI}(x,y,t)$, and $C_{BV}(x,y,t)$.
Choosing properly all the needed parameters and physical models to solve diffusion Equations using Suprem-IV is like driving an airplane. There are hundreds of parameters to choose and optimize to run properly a Suprem-IV simulation. Another challenge in using the legacy software Suprem-IV is that the default values and the default physical models of some parameters have to be changed by the user to include the improved values and the improved physical models found in the recent literature. For example, in Suprem-IV, the charge state of boron ions is assumed to be neutral and singly positive. However, from recent literature, the charge state of boron ions is found to be neutral and doubly positive and not singly positive (Recent). On the other hand, the default values of most parameters in Suprem-IV have been verified for planar CMOS transistors and not for the recent textured solar cells we are working on. For this reason, we are doing our best to digue into the recent experiments found in literature to improve the default values of Suprem-IV parameters.

The theoretical derivation of this pair-diffusion model is described in our previous work (El Boukili 2019: IRSEC) and in (Hansen et al., 1993). A typical set of diffusion Equations for paired boron dopant BI and free interstitial defects I can be written as follows:

$$\frac{\partial C_{BI}(x,y,t)}{\partial t} = -div(J_{BI}) - R \quad (6)$$

$$\frac{\partial C_I(x,y,t)}{\partial t} = -div(J_I) - R \quad (7)$$

Where the fluxes J_{BI} and J_I are given as follows (El Boukili 2019):

$$J_{BI} = D_{BI} C_{BI} \nabla \ln(\frac{p}{n_i}). \quad (8)$$

$$J_I = D_I C_I^* \nabla \ln(\frac{C_I}{C_I^*}\frac{p}{n_i}). \quad (9)$$

However, in this paper, we are taking care of the diffusion of paired and free point defects. In Suprem-IV, to include the effects of the free point defects on the diffusion of paired boron dopant, BI, we need to

include the free points defects concentrations in the flux diffusion Equation (Eq. 8) of paired boron dopant as follows:

$$J_{BI} = D_{BI} C_{BI} \frac{C_I}{C_I^*} \nabla \ln(C_{BI} \frac{C_I}{C_I^*} \frac{p}{n_i}) \qquad (10)$$

The flux of paired boron dopant given by the Equation (10) is more accurate than that given by the Equation (8). The description of all the terms in these Equations from (6) to (10) can be found in (El Boukili 2019) and (Hansen et al., 1993).

5. Results and Discussion

Figure 4 shows the sample of a textured thin film monocrystalline silicon solar cell we are working on. The mesh of this Si(001) structure is generated using Suprem-IV. We have designed this structure so that it will have 3 pyramids. The reason is to prove that the diffusion behavior of boron dopant under the Tips and under the Valleys of the pyramidal textures is completely different. This is an excellent finding in this paper. In the results shown in the following Figures 5 to 12 the implantation dose and energy is 2e+15 atoms/cm^2 and 20 keV respectively. The diffusion time is 20mn for high temperatures and 10mn for low temperatures. Figures 5 and 6 show the interstitial and vacancy defects remaining after diffusion at 400°C, respectively. Figures 7 and 8 show the interstitial and vacancy defects remaining after diffusion at 950°C, respectively. From the Figures 5 to 8, we can say that increasing the diffusion temperature from T=400°C to T=950°C did help minimize the maximum of the densities of interstitial and vacancy defects from 10^{22} to 4.310^{13} and from 10^{22} to 4.810^{15}. Figure 9 shows the boron diffusion profile under the Tip of the pyramid at x=1 um. This Figure also shows that the junction depth under the Tips, J_{depth}^{Tips}, is approximately $0.9um$. Table 4 shows that the junction depth under the Valleys, $J_{depth}^{Valleys}$, is approximately $0.4um$. Table 1 shows the evolution of point defects with increasing temperature. Table 2 shows the evolution of boron dopant and the junction depths with increasing temperature. Table 2 gives the evidence that the optimal high temperature, T_{OH}, is given by $T_{OH} = 950°C$ for the chosen sample structure and the set of implantation and diffusion parameters. We can see from the Table 2 that the junctions' depths and the remaining point defects start increasing when the diffusion temperature is above the optimal temperature $T_{OH} = 950°C$. Then, we can't say that increasing the temperature will always minimize the point defects after diffusion. We need to identify the optimal diffusion temperature T_{OH} for any technology. It is obvious that finding the optimal diffusion temperature from laboratory experiments will be a challenge and expensive. This is evidence that we need to start from numerical experiments to save money and headache. The key finding and discovery in this paper is that when we follow a diffusion with an optimal high temperature T_{OH} by a diffusion with an optimal low temperature T_{OL}, the interstitial and vacancy defects have been reduced significantly from 4.3×10^{13} to 1.02 and from 4.8×10^{15} to 1.09×10^{9}, respectively, see Tables 3 and 4.

On the other hand, the boron diffusion profiles shown in Figures 9 is in excellent agreement with the laboratory experiments and numerical experiments found in (Meyer at al., 2020).

Table 1: Evolution of point defect concentrations.

T	I (defects)	V (defects)
400°C	4.65e+22	4.65e+22
500°C	2.26e+22	3.94e+22
600°C	7.53e+19	1.82e+22
700°C	2.37e+15	5.86e+20
800°C	3.30e+12	2.20e+18
900°C	3.00e+13	1.83e+16
950°C	*4.48e+13*	*4.79e+15*
1000°C	5.21e+13	6.02e+15

Table 2: Evolution of boron dopant and junction depths.

T	B	J_{depth}^{Tips}	$J_{depth}^{Valleys}$
400°C	9.41e+21	0.32	0.18
500°C	9.12e+21	0.35	0.23
600°C	1.89e+21	0.36	0.24
700°C	6.37e+20	0.37	0.25
800°C	2.10e+19	0.40	0.25
900°C	2.22e+19	0.67	0.30
950°C	*2.21e+19*	*0.90*	*0.35*
1000°C	2.05e+19	1.19	0.50

Table 3: Remaining point defects after 10mn cooling down.

Cooldown	I (defects)	V (defects)
100°C	1.02	1.09e+9
50°C	6e-5	3.52e+7

Table 4: Boron dopant and junction depths after 10mn cooling down.

Cooldown	B	J_{depth}^{Tips}	$J_{depth}^{Valleys}$
100°C	3.44e+19	0.9	0.4
50°C	3.44e+19	0.9	0.36

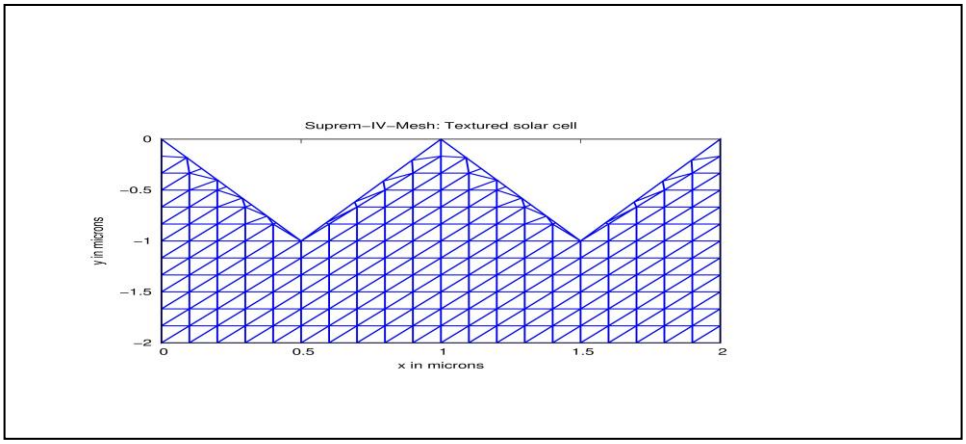

Figure 4: Sample textured solar cell with Suprem-IV mesh.

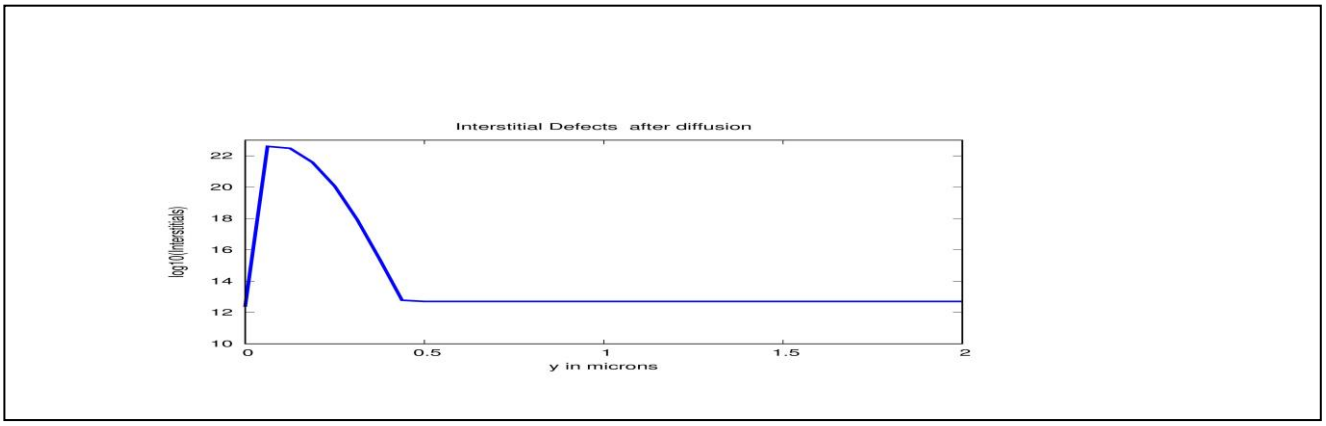

Figure 5: Interstitial defects after diffusion with 400°C.

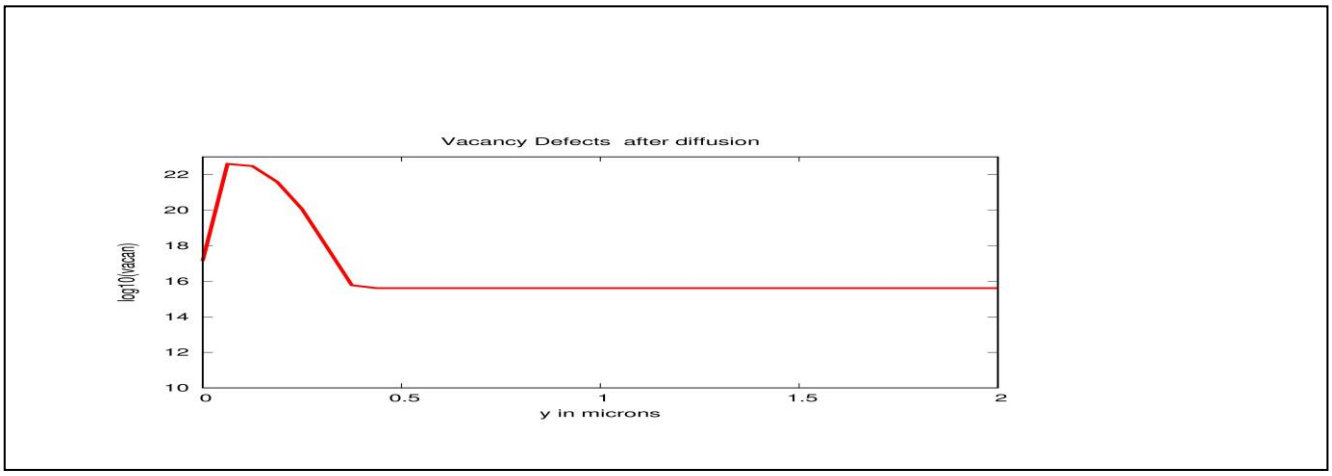

Figure 6: Vacancy defects after diffusion with T=400°C.

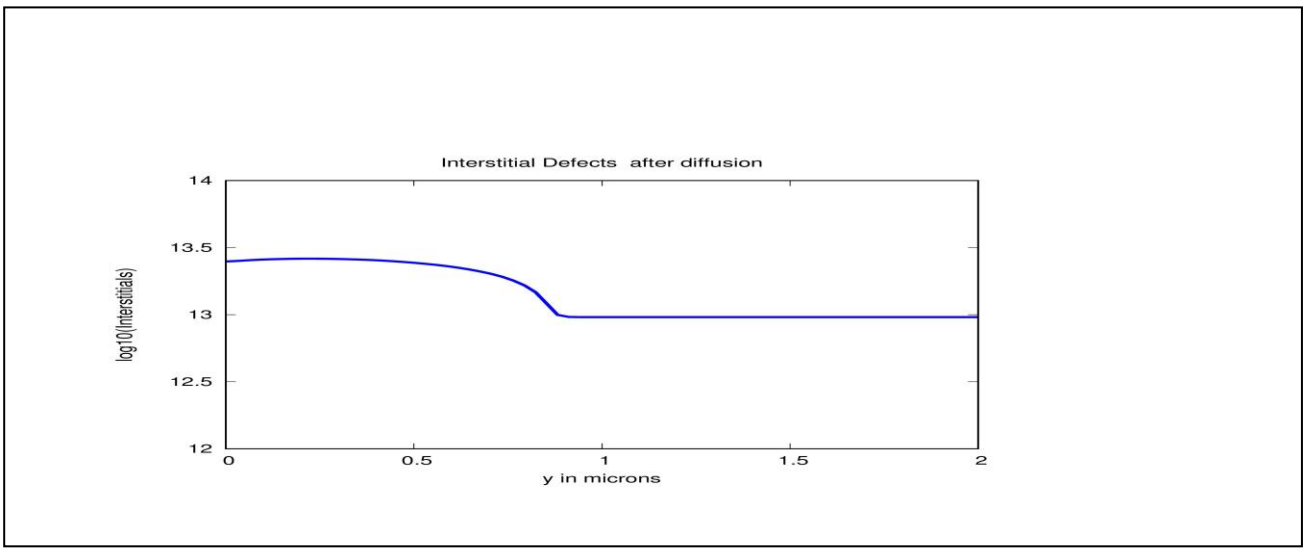

Figure 7: Interstitial defects after diffusion with 950°C.

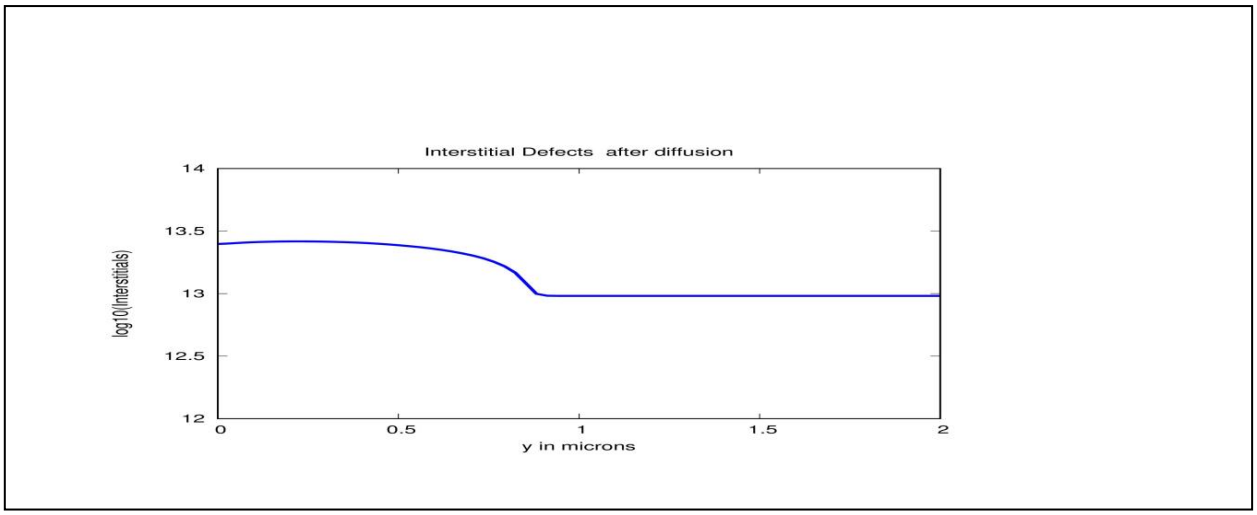

Figure 7: Interstitial defects after diffusion with 950°C.

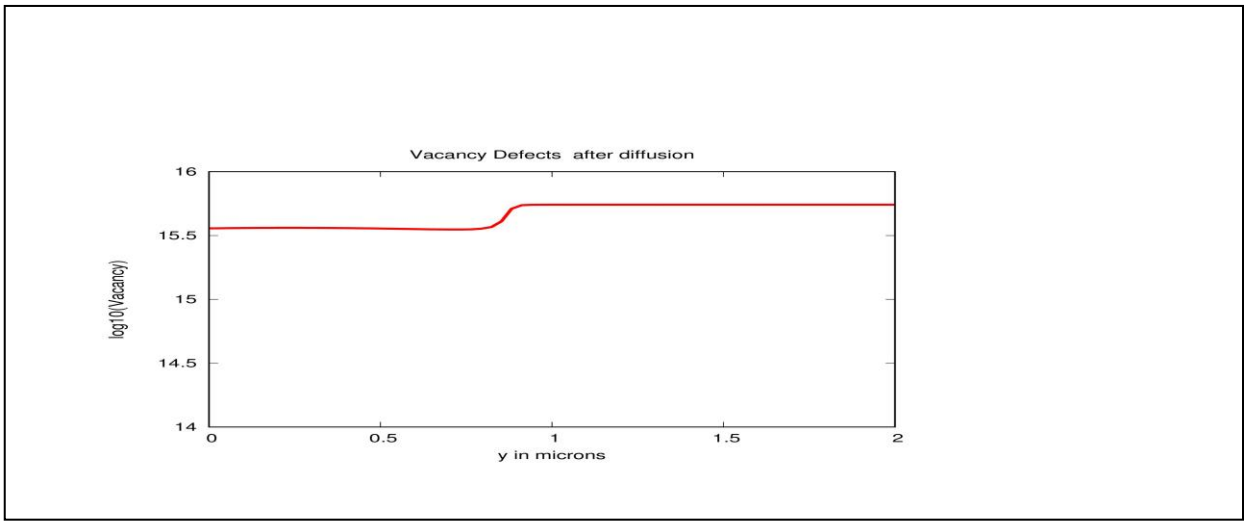

Figure 8: Vacancy defects after diffusion with 950°C.

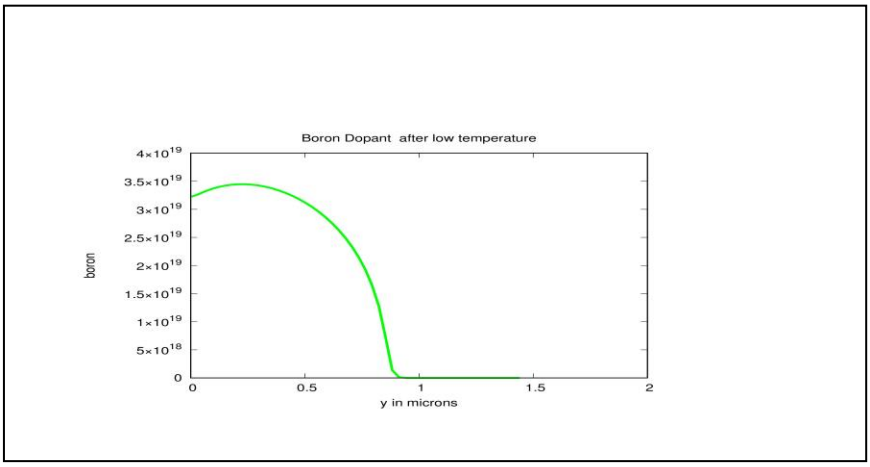

Figure 9: Boron profile after diffusion with 950°C along vertical depth at x=1um.

6. Conclusions

The key findings from the numerical experiments in this research paper are as follows. Firstly, when a thermal diffusion process with an optimal high temperature T_{OH} is followed by a thermal diffusion process with an optimal low temperature, T_{OL}, the remaining interstitial and vacancy defect concentrations have been significantly reduced from 4.3×10^{13} to 1.02 and from 4.8×10^{15} to 1.09×10^{9}, respectively. Secondly, after this process, the dopant profile and junction depths were unchanged. Thirdly, we found that the densities of point defects depend more on the diffusion temperatures, T, than on the ion implantation doses. On the other hand, we found that the obtained results for dopant profiles and junction depths are qualitatively and quantitatively in good agreement with experimental and theoretical results found in recent literature. In the future work, we will investigate the impact of the implantation angles, the screen oxide, and the crystal orientations on the remaining point defects after boron diffusion in a textured thin film silicon solar cell found in the recent market.

References

Rahman, T., Mansur, A.A., Hossain Lipu, M.S., Rahman, M.S.; Ashique, R.H.; Houran, M.A.; Elavarasan, R.M.; Hossain, E. (2023). Investigation of Degradation of Solar Photovoltaics: A Review of Aging Factors, Impacts, and Future Directions toward Sustainable Energy Management. *Energies 2023, 16, 3706.*

Zahi, E., Nadjib, T., Bernards, S., Cedreic, B., Barbara, B., Maurice, Q. (2018). Doping profile measurement on textured silicon surface. *EPJ Photovoltaics Vol. 9, No. 5, pp. 1-8.*

Boyd, C.C., Cheacharoen, R., Leijtens, T., McGehee, M.D. (2019). Understanding degradation mechanisms and improving stability of perovskite photovoltaics. *Chem. Rev. 119(5), 3418–3451.*

Savita, K., Jay, M., Rahul, P. (2019). Design and parametric optimization of ion-implanted PERC solar cells to achieve 22.8% efficiency: a process and device simulation study. *Journal of Sustainable Energy Fuel, 6, pp.3249-3262.*

Jan, K., Tim, B., Felix, K., Xu, J., Puranto, P. (2022). Retarded boron and phosphorus diffusion in silicon nanopillars due to stress induced vacancy injection. *Journal of Applied Physics, 131, 075702.*

Hao, C., Wei, L., Zunke, L., Yang, Z., Dian, M. (2022). Emitter formation with boron diffusion from PECVD deposited boron-doped silicon oxide for high-efficiency TOPCon solar cells. *Solar Energy Materials and Solar Cells, Vol. 240, 111713.*

Krugener, J., Bigie, E., Robby, P., Fabian, K., Tobias, O., Rolf, B., Jorg, O. (2014). Structural analysis of textured silicon surfaces after ion implantation under tilted angle *Semiconductor Science and Technology, 29, pp.1-7.*

Liu, J. (1996). Defect and diffusion study in ion implanted silicon. *PhD Thesis. Department of Materials Science and Engineering of Florida.*

Liang, P., Han, P., Fan, Y., Xing, Y. (2015). Boron implanted emitter for n-type silicon solar cell. *Chinese Physics B, 24(3), 038801.*

Adeline, L., Thibault, D., Coralie, L., Marianne C., Frank, T., Frederic, M., Laurent, R., Sebastien D. (2020). Plasma-immersion ion implantation: A path to lower the annealing temperature of implanted boron emitters and simplify PERT solar cell processing. *Prog Photovolt Res Appl, 2020, pp.2-10.*

Meyer, T., Ehrilich, D., Pichler, P., Titova, V. (2020). Tracing the boron diffusion into a textured silicon solar cell by combining boron diffusion simulation with experimental and simulated scanning transmission electron beam induced current. *www.arxiv.org, 2020.*

Lucio, C., Angelo, B., Piotr, K., Marco, L., Lisa, R. (2019). Silicon solar cells: toward the efficiency limits. *Advances in Physics: X, Vol. 4, No. 1, 1548305.*